



**HAL**  
open science

# Physico-statistical approach to assess the core damage variability due to a total instantaneous blockage of SFR fuel sub-assembly

Nathalie Marie, A. Marrel, J.M. Seiler, Frédéric Bertrand

## ► To cite this version:

Nathalie Marie, A. Marrel, J.M. Seiler, Frédéric Bertrand. Physico-statistical approach to assess the core damage variability due to a total instantaneous blockage of SFR fuel sub-assembly. Nuclear Engineering and Design, 2016, 297, pp.343-353. 10.1016/j.nucengdes.2015.07.012 . hal-03756976

**HAL Id: hal-03756976**

**<https://hal.science/hal-03756976>**

Submitted on 22 Aug 2022

**HAL** is a multi-disciplinary open access archive for the deposit and dissemination of scientific research documents, whether they are published or not. The documents may come from teaching and research institutions in France or abroad, or from public or private research centers.

L'archive ouverte pluridisciplinaire **HAL**, est destinée au dépôt et à la diffusion de documents scientifiques de niveau recherche, publiés ou non, émanant des établissements d'enseignement et de recherche français ou étrangers, des laboratoires publics ou privés.

# PHYSICO-STATISTICAL APPROACH TO ASSESS THE CORE DAMAGE VARIABILITY DUE TO A TOTAL INSTANTANEOUS BLOCKAGE OF SFR FUEL SUB-ASSEMBLY

**N. Marie<sup>1</sup>, A. Marrel<sup>1</sup>, J.M. Seiler<sup>2</sup>, F. Bertrand<sup>1</sup>**

<sup>1</sup> CEA,DEN,DER, F-13108 Saint Paul Lez Durance, France

<sup>2</sup> CEA,DEN,DTN, F-38054 Grenoble, France

## Highlights

- Physico-statistical tool for SFR safety for Total Instantaneous Blockage accident
- 0D/1D but realistic physical models to describe the phenomenological event tree
- 27 uncertain parameters identified to cover all realistic accidental transients
- Uncertainty propagation performed via a Monte-Carlo sampling
- Quantification of safety margins: 18.1% of cases above the safety criterion

## Abstract

Within the framework of the generation IV Sodium Fast Reactors (SFR) R&D program of CEA (French commissariat à l'énergie atomique et aux énergies alternatives), the safety in case of accidents is assessed. These accidental scenarios involve very complex transient phenomena. To get round the difficulty of modelling them, only 'Bounding' (most damaging) accidental conditions have been up to now studied for the safety demonstration. These transients are simulated with very complex multi-physical codes (such as SIMMER) which nevertheless include some adjusted and not well known parameters and require a long CPU (process) time preventing their direct use for uncertainty propagation and sensitivity studies, especially in case of a high number of uncertain input parameters. To cope with these constraints, a new physico-statistical approach is followed in parallel by the CEA. This approach involves the fast-running description of extended accident sequences coupling analytical models for the main physical phenomena in combination with advanced statistical analysis techniques. The efficiency of the methodology for the reactor safety analysis is demonstrated here for one type of accident – the Total Instantaneous Blockage (TIB) – which involves an extended range of complex physical phenomena. From the establishment of the physical models describing the TIB phenomenology, 27 uncertain input parameters and their associated probability distributions are identified. A propagation of these input parameter uncertainties is performed via a Monte-Carlo sampling, providing probability distribution of TIB outputs. A quantification of safety margins is also deduced.

Keywords: Total Instantaneous Blockage, Fast Sodium Reactor, Physico-statistical approach, Safety assessment, Uncertainty propagation.

## Nomenclature

Cp	specific heat	[J kg <sup>-1</sup> K <sup>-1</sup> ]
dt	time step	[s]
Plin	linear power	[W/m]
S	cross section	[m <sup>2</sup> ]
T	temperature	[K]
H	enthalpy	[J/kg]
h	convective heat coefficient	[W. m <sup>-2</sup> K <sup>-1</sup> ]
L	latent heat of phase change	[J/kg]
x	quality	
Z	axial location	[m]
ε	Volume fraction	[-]
ρ	density	[kg/m <sup>3</sup> ]
Φ	heat flux	[W/m <sup>2</sup> ]
b	pool	
c	fuel	
g	clad	
Na	sodium	

# 1 Introduction

Within the framework of the safety of future French SFRs, the demonstration that the risk of propagation of an accident of local melting (such as a TIB) is very low, should be done.

## 1.1 The Physico-statistical approach

From the past, the methodology to demonstrate SFR safety (Database, 2006) was only based on 'Bounding' (or most damaging) accidental scenarios owing to the difficulty of modelling the very complex involved phenomena in a reasonable computational time. The choice to consider a limited number of situations could hide other situations presenting more severe consequences which could be raised during the accident transient. Thus, a new more exhaustive physical approach for the assessment of the safety margins has been developed by CEA. This so-called physico-statistical approach is based on the description of the complete phenomenological event tree with all the possible bifurcations of the accidental scenario with simple (zero or one-dimensional) physical models. The choice of considering simple models is deliberate. Indeed, on the contrary of the complex multi-physic codes (SAS, SIMMER [Kondo et al., 1996]) which require long CPU times for only one calculation, the physico-statistical tool must be able to perform a large number of simulations in a reasonable computational time (few seconds). And, instead of considering physical complex model for each phenomenon, for which a significant body of uncertainty always remains, simple physical models for all phenomena are used in association to uncertainty treatments. The propagation of uncertainties is achieved along the simulations of the transients and the numerous results undergo a statistical treatment to finally highlight the variability of the core damage and assess the respect of safety criteria for all of the possible realistic accidental scenarios. Another benefit of this new approach lies in the possibility to quantify the margins in respect to limit criteria.

In the past, the need of such simplified approaches was also highlighted. Indeed, in the eighties an international consensus (Luck and Bell, 1985; Martin, 1980) was reached that, regarding the complexity of transition phase during SFR severe accident the 'mechanistic' approach is not sufficient to assess safety demonstration. Indeed, the variability and uncertainties associated to the initial conditions, the complexity of physical phenomena with their mutual influence and the sensitivity of the accidental scenario to tiny perturbations limits the credibility of calculation results. In France, a different approach has been developed for PWR severe accident analysis. This approach combines modelling of physical events associated to uncertainties treatment in the LEONAR code (Iooss et al., 2009). In Japan, the methodology development review of Level 2 PSA (probabilistic safety assessment) for SFR (Nakai et al., 2009) underlines the need to consolidate L2PSA studies by analytical methodologies and to construct phenomenological event trees with the determination of all branch probabilities. These authors have also ranked the possible occurring phenomena in various in-vessel and ex-vessel accident sequences and have determined the analytical tools that are necessary to the simulation of each phenomenon. This comprehensive risk evaluation allows also having a feed-back on design for the JSFR (Japan sodium-cooled fast reactor) concept. An analogous approach has also been followed by the IGCAR (Indira Gandhi Centre for Atomic Research) to investigate the core damage due to TIB of a SFR fuel sub-assembly (SA) (Ravi et al., 2013). These authors recognize that, for the elaboration of parametric studies, simplified and robust models that capture the essential features of the event progression are preferable. They develop a robust 1D transient model and investigate the TIB events in PFBR (Prototype Fast Breeder Reactor) fuel sub-assembly with the aim at describing the duration of the various phenomena, estimating the extent of damage propagation. Some sensitivity studies to parameters such as power, hexagonal can (hexcan) wall thickness, thermal conductivity of hexcan material and detection time delay have led to the

conclusion that during the phase at nominal power, damage does not propagate beyond to the first row of surrounding sub-assemblies providing specific design features (holes in hexcans).

Within this context, it has been decided to start the development of such physico-statistical tool and, first, to demonstrate the interest of such approach for assessing and improving SFR safety. An accident that initiates by the Total Instantaneous Blockage (TIB) of a sub-assembly of fresh fuel has been chosen as a reference scenario on the (Super Phenix) SPX core for demonstration purpose before widening this approach. Indeed, experimental results are available for the degradation of this type of core during such TIB transient. This gives information on the physical phenomena and enables partial validation of the tool.

## 1.2 TIB transient

The Total Instantaneous Blockage (Papin, 2012) begins with the arrest of the sodium flow at the inlet of a sub-assembly. Comprehensive investigation of the sequences of events requires the prerequisite establishment of an exhaustive phenomenological event tree considering all possibilities of bifurcations (figure 1).

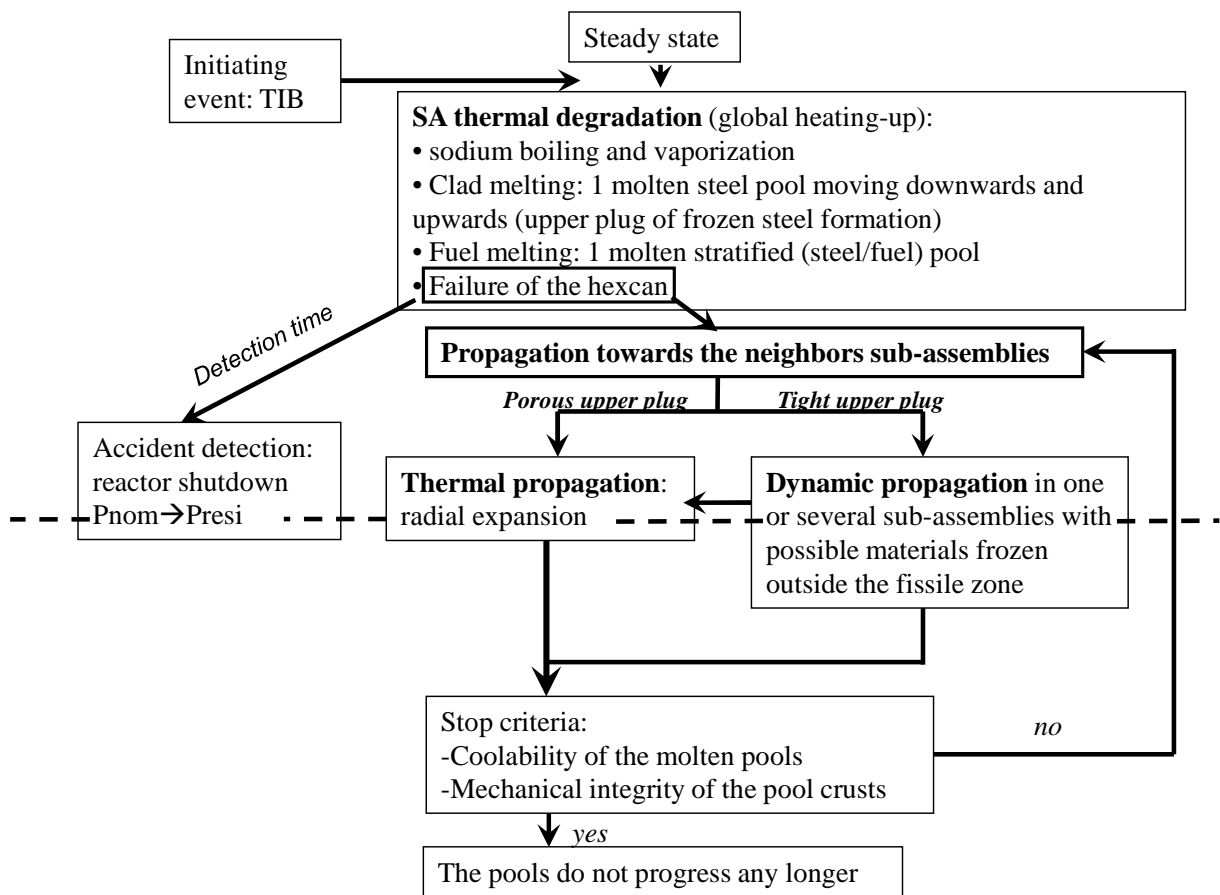


Figure 1 : Phenomenological event tree for TIB accident on a SPX (Super Phenix) geometry

As soon as the SA is blocked, its degradation sequence includes sodium vaporization, dry out, overheating and melting of clad and fuel, formation and motion of the molten pools, and finally, the failure of the hexcan surrounding the blocked SA. Depending on the tightness of the upper plug, that may form when clad melts, the melt propagation to surrounding sub-assemblies can be dynamical or thermal driven propagations (as will be described later), or both types of propagations. In the

following, the modelling assumptions are presented and discussed. Intermediate results are also validated on available experimental results or numerical data. From the establishment of the physical models describing the complete TIB phenomenology, some uncertain parameters and their associated probability density functions are identified (section 2.4). In section 3, some transients corresponding to different sets of uncertain input parameters are highlighted before carrying out an exhaustive uncertainty propagation study in section 4.

## 2 Physical Models

The modelling of successive phenomena occurring during a TIB transient will be described in accordance with the chronological accident progression (figure 1). Since the heat removal rate during a TIB is significantly less than the heat generated, continuous rise in temperature occurs. Indeed, the results drawn from SCARABEE experiments performed with fresh fuels (Kayser et al., 1998) clearly outline that sub-assembly degradation is mainly governed by thermal effects.

During the degradation, the power is supposed to stay at nominal state, which for the Super Phenix reactor corresponds to ~35 kW per pin with an axial heat flux profile of cosine shape. A representative pin/channel is modelled through an axial 1D nodalization. Thus, initial axial average temperature distributions for each pin/channel component (sodium, clad, fuel) are deduced for the initial steady state. The radial temperature distribution in the clad and fuel materials are deduced from steady state heat transfer equations inside the pin. We suppose that the accident is detected by means of DND (Delayed Neutron Detection) only after the onset of propagation in surrounding sub-assemblies, where the flow rate for DNE transport (Delayed Neutron Emitters) is effective. The power falls to residual power only after scram (i.e. ~11 sec after the first hexcan failure).

### 2.1 Blocked sub-assembly degradation

At the beginning of the degradation phase, the heat-up of the blocked SA is quasi-adiabatic. Moreover, evaluating the characteristic time delays for the radial conductive heat transfer through the clad and the fuel pellet, it appears that these characteristic times (0.43 s and 0.74 s, respectively) are small in comparison to heat-up duration of the SA (fuel melting begins around 10 s after the blockage of the flow in the experiment SCARABEE BE3+ (Kayser et al., 1998)). It is thus justified to consider that the radial temperature differences within the pins, at constant power, remains constant versus time before fuel melting. Moreover, from the interpretation of some CESAR experiments with the CASPAR tool (Seiler, 1977; Mercier, 1978), it was concluded that natural convection does not have an important influence on the sodium boiling front progression which is mainly governed by the thermal inertia of the sodium and surrounding structures. This is also confirmed in the IGCAR approach (Ravi et al., 2013) where natural convection of sodium is not considered. Axial conduction is also neglected as in the IGCAR approach.

Thus, the pin locally undergoes a heat-up ( $dT$ ) depending on the local power dissipated in the fuel and the thermal inertia of the whole constituting components (sodium, clad, fuel). For each axial mesh, the following equation holds before sodium boiling:

$$P_{lin}(z) dt = (\rho_c S_c C p_c + \rho_g S_g C p_g + \rho_{Na} S_{Na} C p_{Na}) dT(z) \quad (1)$$

with  $P_{lin}$  [W/m] the linear power dissipation at axial location  $z$  [m],  $\rho$ ,  $Cp$  and  $S$  the density [kg/m<sup>3</sup>], specific heat [J/kg/K], and cross area [m<sup>2</sup>], respectively, of a component ( $c$  stands for fuel,  $g$  for clad and  $Na$  for sodium) and  $T(z)$  is the local temperature [K].

### 2.1.1 Sodium boiling and voiding

The axial evolution of the boiling front is obtained by tracking the location where:  $T_{Na} = T_{Na}^{Sat}$ ;  $T_{Na}$  is the calculated sodium temperature and  $T_{Na}^{Sat}$ , the sodium saturation which, in this case, is taken to 1173K at 1 bar. After boiling inception, the enthalpy of the sodium is further calculated. We consider that dry-out occurs for a specified quality ( $x$ ) corresponding to a given sodium enthalpy elevation  $\Delta H$  [J/kg] such as:  $x = \Delta H / L_{Na}$  with  $L_{Na}$  [J/kg] the sodium latent heat of vaporisation. CASPAR recalculations of the GR-19BP experiment (So, 1984; Papin et al., 1990) well reproduce dry out front evolution for  $x = 0.2$ . Nevertheless, another validation work against CESAR tests shows some uncertainties in the neighbourhood of this value, which may vary from 0.1 to 0.35. Thus, this variable is treated as an uncertain parameter of our model. The time delay associated to sodium voiding and dry out is given by:

$$P_{lin}(z) \Delta t = \rho_{Na} S_{Na} L_{Na} x \quad (2)$$

Once the dry-out is reached, the heat transfer to vapour and the heat to vaporize the remaining quality of liquid are negligible. Thus, the sub-channel is assumed to be sodium voided at this elevation. This hypothesis also has been validated by the interpretation of CESAR experiments (So, 1984). Then, the adiabatic heat-up of the remaining components (clad and fuel) is carried on until the local clad melting criterion is reached.

### 2.1.2 Clad melting and relocation

#### **Clad melting**

The melting front(s) evolutions (from approximately the middle of the fissile length towards the top and the bottom) are given by the axial locations where clad temperature reaches the steel melting temperature (1773 K). Once the steel melting temperature is reached at one axial location, a time delay is associated with clad melting:  $\Delta t = \rho_g S_g L_g / P_{lin}(z)$  (3) with  $L_g$  [J/kg] the clad latent heat of steel. During clad melting, the fuel stays at constant temperature.

#### **Liquid steel relocation**

The volume of the molten steel in the sub-assembly within the clad melting zone undergoes mainly gravity relocation. Indeed, from out-of-pile and in-pile experiments (PELUR, CEFUS, BE3+), the molten steel relocation due to possible entrainment towards the top, of liquid clad by sodium vapour, and freezing in the upper colder zones has been observed and quantified. Furthermore, SCARABEE tests with fresh fuel showed that the sodium vapour flow is not sufficient for a large upward clad entrainment and for tight plug formation (Papin, 2012). This upward entrainment is thus partial and limited, leading to possible porous plugs of small thickness (1cm) in uppermost cold regions. Then, even with these upper plugs, the steel relocation is driven by gravity. In case of higher burn-up fuels, more molten materials could be entrained upwards due to larger fission gas release but only few (CABRI BTI) experimental evidences are available. The molten steel volumes gather at the elevation of the lower clad melting front. Indeed, the PELUR and CEFUS experiments (Papin et al., 1990; Papin et Seiler, 1983) showed that this molten steel freezes at the axial location of the solidus temperature. This relocation results in a stepwise progression of steel accumulation

The upward steel relocation has thus not been modelled in our analytical approach as in the IGCAR approach (Ravi, 2013) but a consequence of a possible formation of upper steel blockage is nevertheless considered in the following. For the stepwise progression of the steel accumulation, a

1D relocation model handles the distribution evolution of the mass of molten steel inside the volumes left free by the sodium. This molten steel forms a downwards moving pool surrounding not molten fuel pins and is supplied by molten steel coming from the axial progression of both upper and lower steel melting fronts.

### Molten steel pool heat-up

This specific region of the degraded SA, where a liquid steel pool surrounds the fuel pellets, is treated with a 0D transient approach (figure 2) coupled to the previous 1D modelling which allows determining the pool location. The heat losses in the axial direction are neglected (Ravi, 2013). Heat transfer takes place predominantly in the radial direction from the pool towards the hexagonal wrapper and thus the blocked SA heating-up becomes no more adiabatic.

In this zone of solid fuel pellets surrounded by a steel pool (figure 3), two thermal balances are written: on one hand on the solid fuel and on the other hand on the molten steel. The power release by the fuel contributes to the steel heat-up and is transferred to the steel pool through a global heat transfer coefficient which stands for the radial conduction inside the fuel pellets and for the convection within the steel pool. Finally, the steel pool loses power by convection towards the hexcan.

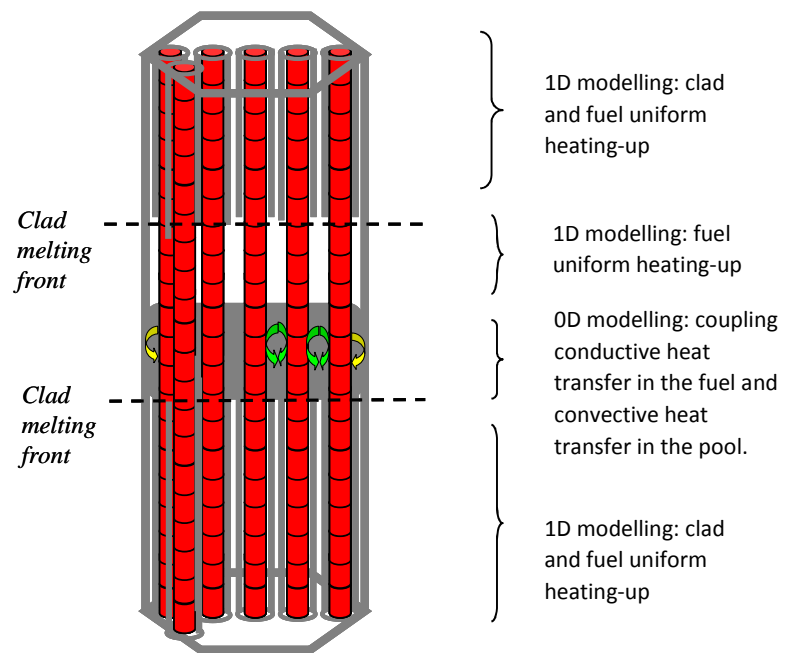


Figure 2 - Graphical representation of the faulted sub-assembly during the accidental transient beyond clad melting phase

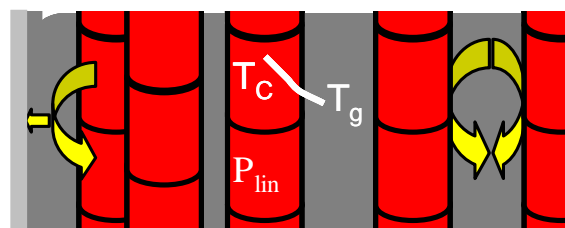


Figure 3: Graphical representation of molten steel pool around the fuel pins.

### ***Fuel adiabatic heat-up***

The region of the SA where the molten steel has disappeared is still treated with the previous 1D approach (figure 2). The fuel pellets are assumed to stay in place and undergo a quasi-adiabatic heat-up until the local fuel melting is reached.

### **2.1.3 Fuel melting and relocation**

#### ***Fuel melting***

As for the steel, the melting front(s) evolutions are given by the axial locations where fuel temperatures exceed the fuel melting temperature. An average value of 3006K is taken for this melting temperature between the solidus and liquidus temperatures. No uncertainty has been associated to this value because the difference between these two temperatures is only of around 200K but this can be done in further evaluations. Once this criterion is reached at one axial location, the fuel is supposed to melt coherently. This assumption permitted to well reproduce fuel melting during the SCARABEE BE3+ test (Papin et al., 1990). The local fuel melting delay is similarly given by an energy balance on the fuel, as equation (3) applied to fuel.

#### ***Molten fuel relocation***

As for molten steel, the volume of the molten fuel in the sub-assembly is instantaneously relocated by gravity at the elevation of the lower fuel melting front (SCARABEE BE+ tests). The 1D relocation modelling permits to follow the fuel pool relocation. The clad above the molten fuel pool, which is molten after the creation of the fuel pool, forms an upper molten steel layer owing to the density difference with the fuel (figure 4). Furthermore, once the lower fuel melting front penetrates into the lower steel pool, the steel previously contained within this penetration zone instantaneously relocates in the upper molten steel layer.

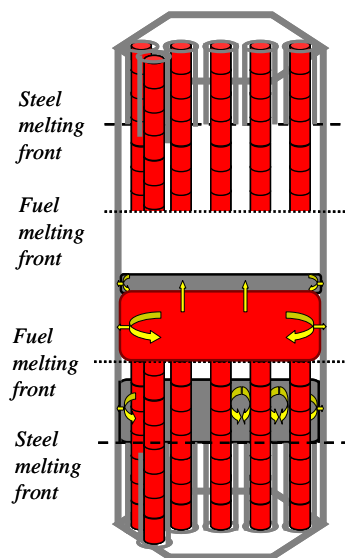


Figure 4 - Graphical representation of the faulted sub-assembly during the accidental transient beyond clad and fuel melting criteria

#### ***Molten pool heat-up***

Different zones involving various heat transfer mechanisms appear between upper and bottom fuel melting fronts (figure 4): a cavity empty of material and a zone with two separated molten layers (pools) (figure 5).

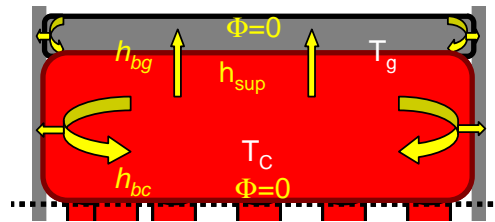


Figure 5 - Graphical representation of upper molten steel pool and the fuel pool

In this zone, a second 0D modelling involves two new thermal balances written on each separate pool. The main physical assumptions, validated on past experimental works, are the following:

- The pools are surrounded by their own crust (material at its melting temperature), as observed from post-test examinations of SCARABEE 3 (Kayser et al., 1998), and the fuel melting temperature being higher than the steel one, the crust separating both pools is assumed to be made of solid fuel.
- The convection regime at the top of the fuel pool results from Rayleigh-Benard instabilities and the heat transfer coefficient is derived from (Bernaz, 1999).
- The heat transfer towards the lateral surfaces depends on the convection within the pools; Alvarez et al. (Alvarez et al., 1986) derived, from BAFOND experiments, an average Nusselt number over the pool height in laminar or turbulent regimes for a cylindrical pool. For boiling pools, the Greene et al. (Bede et al., 1993) correlation (validated on SEBULON data) is used. Because some uncertainties remain on these correlations (linked to experimental discrepancies, to fast transient effects and effect of real materials...), the Nusselt numbers are considered as uncertain.
- The heat flux towards the bottom interface of the fuel pool is neglected in accordance with BAFOND experimental evidence because of thermal stratification at the bottom. These heat losses are also neglected by Ravi et al. (Ravi, 2013).
- Finally, the heat flux across the upper surface of the steel pool is neglected. Radiation heat transfer is neglected in this preliminary demonstration as by Ravi et al. (Ravi, 2013) but could be taken in account in future studies

#### 2.1.4 Degraded SA hexcan failure

The mechanism leading to the hexcan failure is complex and has been interpreted as thermal erosion linked to fuel crust instability (Papin, 2012). Experiments (Kayser and Soussan, 1991; Dadillon, 1990) showed that the hexcan could be deformed and, due to the possible over-pressure in the SA, could touch the wrapper of the surrounding hexcans. Thus, depending on conditions (over-pressure, local mechanical defaults or hot points within the wrapper ...), the failure may be caused by combined thermal and pressure effects. To encompass the various failure modes, the hexcan is assumed failed as soon as a given fraction of its thickness is molten. This fraction is treated as an uncertain parameter. The hexcan failure initiates the propagation process. At the hexcan failure instant, variables are evaluated with the aim of initiating the melt propagation process.

## 2.2 Propagation

The propagation phenomenology of the molten materials towards and inside the neighbouring SAs has largely been discussed in the past. Livolant et al. (1990) showed from SCARABEE PVA evidences that experimental results are between results obtained in case of either only a thermal propagation

or only a hydrodynamic one. Thus, the propagation model will be a combination of these two modes. Thermal propagation is a propagation process controlled by the heating up and melting of the invaded structures. Hydrodynamic propagation supposes that the movement of ejected materials is only controlled by hydrodynamic effects; i.e. due to pressure difference between the faulted SA (possible pressurisation due to vaporization of the trapped materials associated to a tight upper plug or, after the failure, local fuel-coolant interaction (FCI)) and their neighbours. From past experiments, some physical understandings have been derived: the higher this pressure difference, the less isotropic the propagation. For low pressure differences, there is no hydrodynamic propagation but only a thermal propagation which is in average isotropic, owing to the very high temperature of the molten pool. However, there remains a lack of data to quantify the relation between this pressure difference and the number of neighbour SA affected by hydrodynamic propagation. Thus, this number is considered as an uncertain parameter.

After hexcan failure and a first phase of hydrodynamic propagation towards the neighbour SAs, this over-pressure vanishes and the remaining structures in the neighbouring SAs undergo only thermal propagation. Also, based on the main conclusions of the SCARABEE-N program (Livolant et al., 1990), which have highlighted that a TIB accident does not lead to violent energetic FCI and to the destruction of the SA, only effects of mild local FCIs are taken into account promoting hydrodynamic propagation. Violent energetic FCI could lead to other transient progressions which could be added to the present phenomenological tree in future developments.

Thus, several configurations of propagation will be encountered:

- only an isotropic thermal propagation toward the 6 neighbouring SAs,
- or a first phase during which a given number of neighbouring SAs (given by an uncertain parameter) undergo a hydrodynamic propagation, followed by a second phase where the thermal propagation goes on in all the six neighbouring SAs.

Furthermore, The SCARABEE BE 3+ and PIA tests confirm that no significant amount of fuel escapes through the inter sub-assembly gap due to early hexcan deformation and inter-sub assembly blockage formation.

In the following, the modelling of the accident progression in case of hydrodynamic or thermal propagation is described.

### 2.2.1 Hydrodynamic propagation

According to literature (Papin, 2012), the ejection of the molten material from the faulted SA, consequently to an over-pressurisation, is achieved through a succession of mild molten material progressions. This invasion of the hot molten material leads to melting of the trapped fuel pins and formation of new crusts straight after ruined by local mild Fuel Coolant Interaction (Kayser and Soussan, 1991). The delay of the hydrodynamic propagation corresponds to the time required for the hydrodynamic penetration of the whole inventory of ejected molten material. This mass is evaluated, at the hexcan failure time, as the mass of molten steel in the upper pool and the molten fuel mass that is located above the failure location. The failure is assumed to occur at the maximum heat flux location as observed experimentally (Papin et al., 1990). This location of the maximum heat flux ( $Z_{pic}$ ) is treated as an uncertain parameter whose average value is derived from axial heat flux profile of SCARABEE BF2 and BF3 experiments (Bede et al., 1993). The shape of the relocated volume within the neighbour sub-assemblies is deduced from experimental evidences from the SIGELCO radial melt injection experiments (Duret et al., 1988), which provides the aspect ratio treated as an uncertain variable ( $k_{sig} = H_{sig} / X_0$  with  $H_{sig}$  the axial penetration distance and  $X_0$  the radial one ). By

assumption, the volume of relocated material is centred on the failure location ( $Z_{rup}$ ). Thus the other features (the height  $H_{sig}$  and the radial penetration  $X_0$ ) are deduced from the shape of the occupied volume (hexagonal radial surface and height of  $H_{sig}$  - figure 6) and the volume relocated.

At the time of fuel penetration into neighbour subassemblies, the delayed neutrons are transported by the sodium flow and can be detected. The uncertain parameter  $t_{DND}$  (Delayed Neutron Detection) is the duration required to detect the accident and activate the reactor shutdown after the hexcan failure ( $\sim 11s$  considered in EFR safety report). Beyond this time delay, the power shifts to residual power and the decrease law of this residual power in the SPX reactor is considered. After the penetration of molten materials inside the neighbouring SA, the time delay required to heat up and melt the pins trapped within the invaded volume is calculated (the heat leading to sodium vaporisation being negligible), taking into account the evolution of the core power.

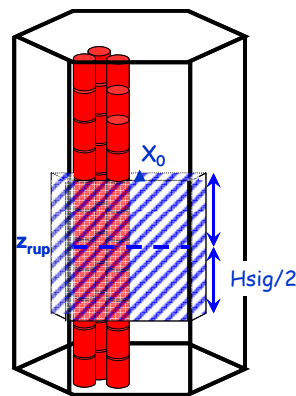


Figure 6 - Occupied volume by the ejected molten mass in a neighbour SA affected by hydrodynamic propagation

### 2.2.2 Thermal propagation

The following covers simultaneous phenomena as illustrated in figure 7: the continuation of the axial degradation of the faulted sub-assembly after hexcan failure and the radial thermal progression of the molten material in neighbour SAs.

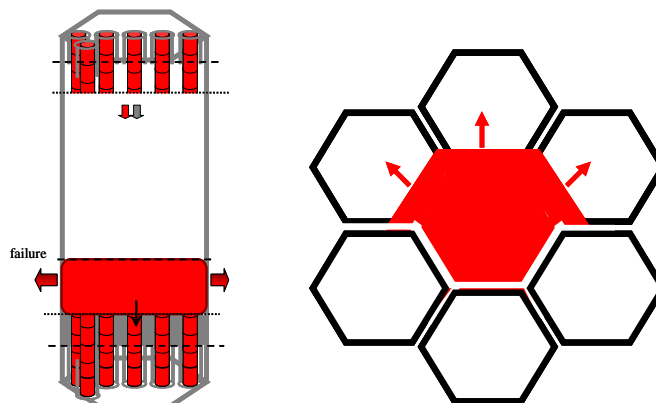


Figure 7 – Thermal propagation and of the extended pool gathering the faulted SA and the three sub-assemblies only concerned by thermal propagation.

For the description of thermal propagation, it is assumed that all the power dissipated in the molten materials serves to heat up and melt the surrounding structures in the neighbour subassemblies (figure 8). The molten materials at melting temperature are then mixed in with the pool leading to a decrease of its temperature.

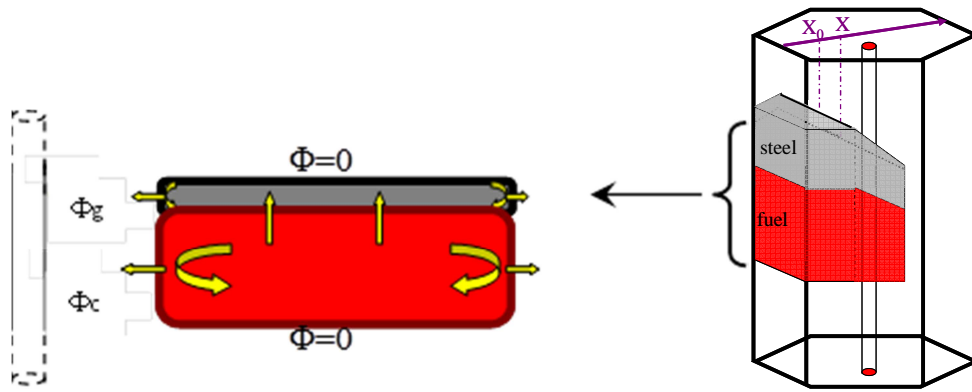


Figure 8: Graphical representation of the molten material progression

## 2.3 Pool Unification and accident end criteria

### 2.3.1 Pool unification

Once the trapped pins during the hydrodynamic propagation are molten, the molten materials are gathered in one cylindrical stratified pool keeping masses (material total volumes), energy (resulting in new pool temperatures) and the lateral surfaces for purpose of further thermal propagation.

### 2.3.2 Accident end criteria

Three criteria must be fulfilled in order to reach the end of the accident:

*The final corium configuration should be coolable:*

1. i.e. in residual power, after the scram,
2. in each neighbour sub-assembly, the maximum sodium temperature (sodium located nearby the pool crust) should remain below the sodium boiling temperature. This local maximum temperature is calculated from radial heat flux coming from the molten pool, the local bulk temperature of sodium flowing in the neighbour SAs and the convective heat transfer coefficient of Lyon (Lyon, 1949). The sodium velocity nearby the pool crust is taken as an uncertain parameter

*The final corium configuration should be mechanically stable:*

3. in each neighbour SA, the crust thickness should be sufficient to prevent crust rupture, i.e. the crust thickness should be greater than a critical thickness (uncertain parameter  $e_{crit}$  of median value 2.5mm from SCARABEE post-test examinations). If it is not, it is assumed that, even if the preceding criterion is fulfilled, that the crust will fail and the melt propagation will go on. The crust thickness is evaluated from a steady state approach assuming that the heat flux released by the pool is evacuated by conduction through this crust thickness.

## 2.4 Uncertain Parameters

In this preliminary demonstration of this physico-statistical tool, 27 uncertain parameters are highlighted. Certainly, some others could be studied in future studies. These uncertain parameters fall into two categories: epistemic or aleatory (Der Kiuregian, 2007). The first type of parameters gather those related to *the core configuration and reactor features*, for which a lack of knowledge still remains, such as:

- the assembly power and sodium velocity within the neighboring SA depending on its location within the core as well as its burn-up,

- the material properties whose uncertainties lie not only in the lack of knowledge due to the difficulty of high temperatures measurements but also in the state of the core (fuel burn-up, ...),
- the unknowns associated with the void fraction in the boiling pools,
- the time delay for delayed neutron detection associated with the core instrumentation and flow path,
- the lack of physical knowledge regarding the mechanisms which lead either to thermal or hydrodynamic propagations of molten materials,
- the acceptable values for the minimum crust thickness guaranteeing the mechanical stability of molten materials,
- the unknown concerning the type of propagation (thermal or hydrodynamic) which should be related to pressurisation of the damaged SA. And if the propagation is hydrodynamic, the ignorance of the number of affected SA.

The second type of uncertainties is related to *physical models* described above and for which probabilistic distributions are derived from experimental data:

- the uncertainties associated to models based on some experimental data derived from specific experiments are considered: the specified dry out quality correlated from CASPAR results and GR-19 BP experiment, the aspect ratio of the ejected material relocation shape in hydrodynamic propagation from SIGELCO experiment, the failure localization over the pool height from SCARABEE post-test examinations...

The uncertainties around heat transfer coefficients correlated from experimental tests performed with simulant fluids and the associated correlated Nusselt numbers.

The quantification of variable uncertainties is performed either by using a statistical modelling based on the analysis of available data (for aleatory variables), or by expert judgment (for epistemic variables). At the end of this step, 27 independent uncertain variables have been defined for the TIB test-case and their probability density functions are given in table 1.

Definition	Probability distribution	Distribution parameters			
		P1	P2	P3	P4
<b>Input data and physical properties</b>					
1) SA Fuel power variation (burn-up) [W]	Truncated normal	0	0.04	-0.34	0.21
2) Density of fuel [kg/m <sup>3</sup> ]	Triangular	7220	8740	1080 0	
3) Density steel [kg/m <sup>3</sup> ]	Triangular	5820	6800	7960	
10) Density of sodium [kg/m <sup>3</sup> ]	Uniform	750	870		
4) Heat capacity of fuel [J/kg/K]	Uniform	380	500		
5) Heat capacity steel [J/kg/K]	Uniform	600	800		
11) Heat capacity of sodium [J/kg/K]	Uniform	1200	1400		
6) Conductivity of fuel [W/m/K]	Uniform	2	5		
7) Conductivity of steel [W/m/K]	Uniform	10	20		
8-9-12) Latent heat variations for fuel (average: 2.82 10 <sup>5</sup> ), for steel (average: 3 10 <sup>5</sup> ), for sodium (average: 3.86 10 <sup>6</sup> ) [J/kg]	Truncated normal	0	0.1	-0.2	0.2
<b>Modelling variables</b>					
13) Quality at dry-out occurrence (x eq. 2 (So et al. 1984)) [-]	Truncated normal	0.22	0.076	0	0.8
14-15) Void fraction in boiling pools of fuel, of steel, respectively (if empty volume remaining) [-]	Uniform	0.01	0.99		

<b>16-17-18-19-20)</b> Nusselt number variations around the value given by the correlations of Alvarez (1983) for steel and for fuel, of Greene (Bede,1993) for steel and for fuel, and finally of Lyon (1949) for sodium.	Truncated normal	0	0.2	-0.6	0.6
<b>21)</b> Time delay for delayed neutron detection [s]	Triangular	9	11	30	
<b>22)</b> Fraction of the hexcan thickness to melt before failure [-]	Triangular	0.5	1.5	2	
<b>23)</b> Aspect ratio of the form taken by the ejected material in hydrodynamic propagation. From SIGELCO data : [8,3 6,8 8,8 8,3] (Duret, 1988)	Truncated normal	8.05	0.866	1	10
<b>24) Propagation mode :</b> Number of neighbor SAs affected by hydrodynamic propagation	Discrete Uniform (entire value)	0	6		
<b>25)</b> Fuel pool height underneath the failure location over the total pool height [-] (SCARABEE BF2, BF3) (Papin, 1990)	Triangular	0	0.75	1	
<b>26)</b> Critical crust thickness (mechanic stability) [mm]	Triangular	1	2	5	
<b>27)</b> Sodium velocity in the neighbor SA [m/s] (coolability criterion)	Triangular	2	7	20	

With :

Probability distribution	Parameter P1	Parameter P2	Parameter P3	Parameter P4
Uniform	Minimal value	Maximal value		
Triangular	Minimal value	Modal Value	Maximal value	
Truncated normal	Mean	Standard deviation	Minimal value	Maximal value

Table 1: Uncertain inputs parameters and their associated probabilistic model

For this preliminary demonstration, it has been considered that the thermal propagation (e.g. any neighbouring SA affected by hydrodynamic propagation) and hydrodynamic propagations in the various numbers of SA are equiprobable. Further studies would be carried out to assess the influence of these hypotheses on the predicted safety criteria.

### 3 TIB simulation Results

Before carrying out a systematic treatment of effects of uncertainties for TIB accident, results obtained for different sets of uncertain parameters are described and compared to existing data.

#### 3.1 Results for reference values of uncertain parameters

The results of this degradation phase obtained with the mean value of the 27 uncertain parameters are analysed, based on the observation of various front progressions. Sodium boiling and dry-out, clad and fuel onset and end of melting (figure 9) are consistent with the results of the validated MADONA analytical approach (CEA tool) obtained in SPX configuration and with SCARABEE BE3+ experiment (a 37 pins bundle). This test evidences the realistic sequence of the degradation of the faulted sub-assembly under TIB conditions which lasts over 14-16s assuming nominal power conditions. From experimental evidences (Kayser et al., 1998) sodium boiling begins at 2 s near mid-plane (a little bit later in our results –fig 9) and propagates upwards and downwards. Steel clad melting occurs around 5-6 s (compared to 7-8s in figure 9), fuel melting at 8-14 s (in good agreement with fig. 9) and hexcan fails at 21.5 s in front of the boiling fuel pool (compared to 20.07s with our calculation). Finally these results are already very close to experimental results.

The result of the propagation phase is much more difficult to assess because no integral well instrumented experimental test with propagation inside the six neighbour SAs exists. Only the SCARABEE-PVA test exists at a very smaller scale (Dadillon, 1990). It has nevertheless demonstrated that two kinds of propagation types could occur (thermal or hydrodynamic).

The summary of the phenomenology of the propagation phase simulated by our TIB simulator, still considering average input variables, is described in the following. After hexcan failure at 20.07s, 3 neighbour SAs are invaded by hydrodynamic propagation (test case hypothesis); the three remaining SAs are invaded by thermal propagation. The heat-up and melting of pins trapped within the melt in SAs undergoing hydrodynamic propagation last 12.6s, thus the gathering of pools issued of hydrodynamic propagation with the pool in thermal expansion occurs at  $t_{unif}=32.67s$ , whereas the instant of scram is  $t_{AU}=35.6s$ . Finally, the accident end criteria are reached at 298 s and the final equivalent numbers of molten SAs is  $nbMSA=4.905$  (i.e. Mass of molten fuel over fuel mass of one SA).

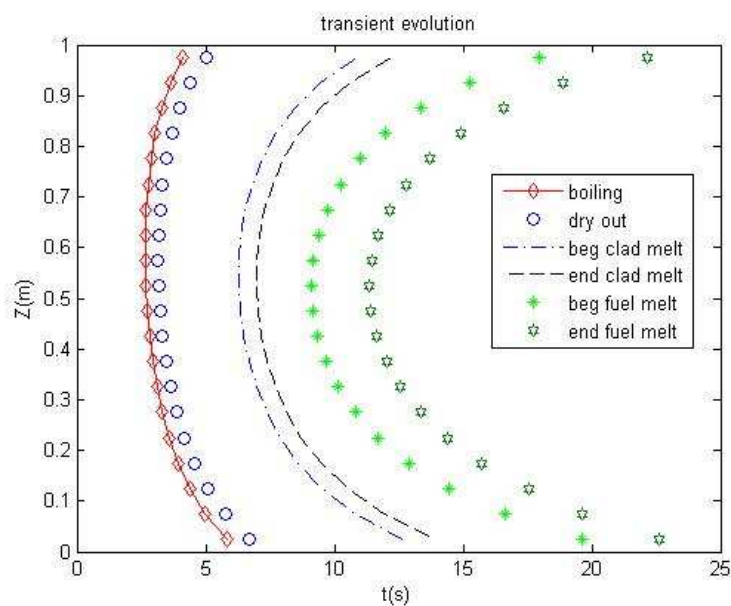


Figure 9: Progression of the various fronts: sodium boiling, dry-out, clad and fuel beginning and end of melting.

### 3.2 Results for some other sets of uncertain parameters

Five different cases have been selected to illustrate the various transients following the blockage of a SA. In figure 10 is displayed the evolution of molten fuel masses along the transient in case of various set of uncertain parameters. The associated characteristic times of the transients are given in Table 2. On the left side of this figure the whole transient is displayed whereas the left side is a focus on the 150 first seconds.

1. The case 1 is obtained with a set of uncertain parameters among which the fuel power variation is -0.25 (thus the power is 0.75 times the average power over all the realistic power SA and this power remains constant until the accident detection), the number of neighbour subassemblies affected by hydrodynamic propagation is zero and thus the pool undergoes only thermal propagation and the sodium velocity at the bottom of the neighbouring SAs is 4.64 m/s (to evaluate the possible coolability of the molten pool). This latter has an impact on the end of thermal propagation. As the power is low, the fuel melting starts lately  $\sim 15s$ . The molten mass increases with the melting of the blocked sub-assembly. This SA failure

occurs at 29.1s and the reactor scram at 37.7s (table 1). After that time the slope of the curve in figure 10 changes owing to the decrease of power to residual power. The equivalent mass of seven molten SA is reached at 1457s. As the sodium velocity is low in the surrounding SAs, the heat released by the pool could not be removed by this sodium flow. As the pool propagation progresses, it gets colder because the residual power decreases, the heat losses through its enlarging top surface increase and molten materials at melting temperature are continuously incorporated. The lateral heat from the pool drops and the cooling criterion is reached at 4550.48s. At that time the final equivalent numbers of molten SAs is  $nbMSA=22.73$ .

2. The case 2 is obtained with another set of uncertain parameters. In this case, the SA power is the average power, none neighbour SA is affected by hydrodynamic propagation (only thermal propagation occurs) and the sodium velocity in the no-affected sub-assemblies is higher: 14.08 m/s. In figure 10, the fuel melting starts earlier and, as the shut-down occurs later (39.01s), the fuel mass melted in this first part of the transient is much more important (equivalent mass of 7 molten SAs obtained at 1457s). However, the cooling criterion is reached earlier (1776.74s) and the final  $nbMSA$  is 20.37.
3. In case 3, the fuel melting starts later because the SA power is 0.7 times the average power, the rupture of the SA occurs at 24.22s and is followed by an invasion of 4 surrounding SAs in hydrodynamic propagation. The reactor scram occurs at 53.36s and, at that time, the cooling criterion for the pool in thermal propagation is fulfilled. However the material trapped in the invaded zones are completely melted at 45.5s and this molten material gathers the pool which progress in thermal expansion until the cooling and mechanical holding criteria are verified. The final  $nbMSA$  is only 5.41.
4. In case 4, the SA power is 1.16 times the average power, the melting starts early and the hexcan failure occurs at 16.61s. In this case, the hydrodynamic propagation affects 2 surrounding SAs but the materials trapped melt (29.2s) before the scram (32.61s). The cooling criterion is fulfilled at that time whereas the mechanical holding criterion is reached only 12.26s later and the  $nbMSA$  is only 2.67.
5. The last case 5 which gives the lowest  $nbMSA$  (1.13) is obtained for a low SA power and a hydrodynamic propagation affecting all the surrounding SAs. The material trapped is completely molten (at 204s) much later than the scram (35s) and the transient stops on the fulfilment of the mechanical holding criterion at 206.6s.

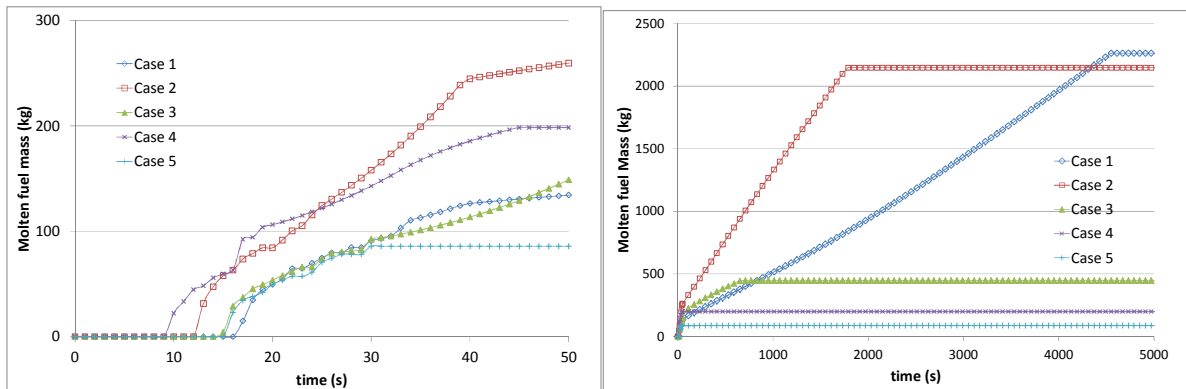


Figure 10: Evolution of molten masses in case of five various set of uncertain parameters (zoom on the left).

	<i>nbMSA</i>	<i>time at hexcan failure (s)</i>	<i>time at pool unification (s)- t<sub>unif</sub></i>	<i>time when 7 equi. SAs are molten (s)- t<sub>crit</sub></i>	<i>time of reactor scram (s) – t<sub>scram</sub></i>	<i>time when thermal arrest criterion is reached (s)- t<sub>Na</sub></i>	<i>final time (s) - t<sub>final</sub></i>
Case 1	22.72	29.08	-	1457	37.71	4550.48	4550.48
Case 2	20.37	20.23	-	473.61	39.08	1776.74	1776.74
Case 3	5.41	24.44	45.5	-	53.56	53.57	664.38
Case 4	2.67	16.61	29.2	-	32.61	32.61	44.87
Case 5	1.13	24.46	204	-	35	204	206.06

Table 2: Associated *nbMSA* and characteristic times of the transients in case of the five various set of uncertain parameters.

#### 4 Uncertainty propagation Results

The propagation of input uncertainty has been performed via a Monte-Carlo sampling (Gentle, 2003) of 1000 TIB simulations, following the probability distributions given in Table 1. These 1000 simulations have been performed with a relatively low CPU cost of around 6 hours. The elementary statistics of the corresponding predicted outputs are summarized in table 3. The repartitions of the final *nbMSA* and characteristic transient times ( $t_{crit}$ ,  $t_{unif}$  and  $t_{final}$ ) are given by figure 11.

Thus, from table 3, it comes that the mean output of a TIB on a type SPX SA is 5.5 final equivalent molten SAs with a standard deviation of 7.5, which attests to the relatively large variability of the predicted final *nbMSA* (ranging from 1.02 to 37 molten SA). The observed distribution of the final *nbMSA* is unimodal and clearly asymmetric, with a right skew: the right tail of the distribution is longer, most values are concentrated on left of the mean, with extreme values to the right. Consequently, the values lower than the mean value are more frequent than the higher, as it is confirmed by a median value (i.e. the 50<sup>th</sup> percentile) of 2.6. Figure 2 also illustrates that, in most of cases a TIB would not exceed the safety criterion of 7 molten SAs, value taken to prevent general core melting (EFR Report, 1999). The empirical probability of having a final *nbMSA* upper than 7 is estimated on the Monte-Carlo sampling; the obtained value is 18.1%. In a safety framework, this fraction of overall cases should be reduced in order to reinforce the reactor safety. That is why it is worthwhile to identify, via a sensitivity analysis, the uncertain parameters which are the most influential on the predicted final *nbMSA* and which lead to such critical configurations. The sensitivity analysis is presented in another paper (Marrel & Marie, 2014).

	<i>Final nbMSA</i>	<i>t<sub>crit</sub> (s)</i>	<i>t<sub>unif</sub> (s)</i>	<i>t<sub>final</sub> (s)</i>
Mean	5.5	459	49.9	331.3
Standard deviation	7.5	201.9	32.8	582.5
Median	2.6	417	35.3	85
Min	1.02	116.4	22.5	25.8
Max	37	1217.1	210.6	4552

Table 3: Summary statistics of TIB outputs (same legend as table 2).

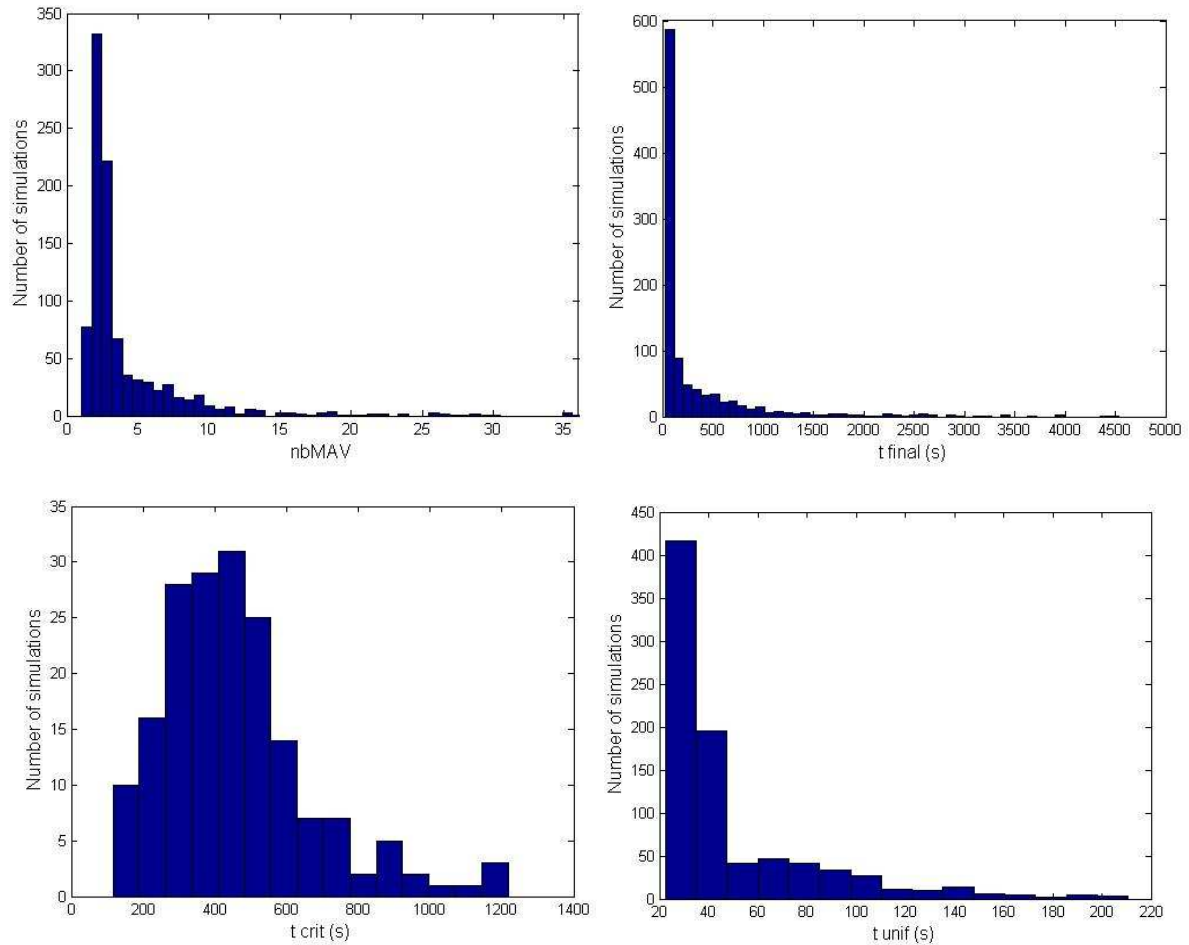


Figure 11: Probability distributions of TIB outputs, nbMAV,  $t_{final}$ ,  $t_{crit}$  and  $t_{unif}$ .

From table 3 and figure 11, it also appears that, even if TIB transients last from 26 s to more than one hour, a TIB transient lasts in average 331s. The statistics given in table 3 for the time when 7 SA are molten ( $t_{crit}$ ) are restricted to the 18.1% of cases for which this safety criterion is reached. This safety criterion of 7 nbMSA is reached within the range of 2 - 20 minutes and in average at 7min39s. On the same way, only transients including pool unification are considered for establishing the distribution of the time  $t_{unif}$ , which consist in 85.7% of simulations of TIB transients. From table 3, the pool unification occurs very quickly. Figure 11 shows that in most cases the pools gathers between 20 and 50 s (median at 35s).

Further sensitivity analysis studies on the characteristic transient times are performed in Marrel & Marie (2014) and main conclusions regarding the way of improving the reactor safety are derived.

## 5 Synthesis

The final main objective of this work is to demonstrate the potential of calculation tools combining analytical physical modelling with statistical treatment of uncertainties for assessing the safety of SFR reactors. This approach, which should be considered in parallel of the previous traditionally 'Bounding' approach, is developed to cope with the broad multiplicity of accident paths and complex phenomena that characterize core degradation of SFR accidents. This approach implicitly takes into account that the available analysis tools can only approximate the physics of SFR core degradation and that the available experimental and theoretical information for model verification are limited.

As a preliminary evaluation of the efficiency and interest of such a physico-statistical tool, the accident initiated by a TIB of a SA at nominal power (assumed without important neutronic feedback) of the SPX (Super-Phenix) core type with fresh fuel is chosen for demonstration purpose before widening this approach to other accidental scenarios and geometries. A TIB starts with the flow blockage of one SA. Various thermal-hydraulic phenomena taking place during degradation of the blocked SA and the radial propagation of damage to the neighbor SA are very complex, involving phase change heat transfer, moving solid-liquid interfaces and progressive changes in the geometrical configurations of the blocked and surrounding SA as a consequence of melting of fuel, clad and hexcan. A comprehensive investigation of the sequences of event progressions is displayed through a phenomenological event tree considering the associated possibilities of bifurcations between various accident progression modes. As soon as the SA is blocked, its degradation spreads out from the sodium vaporization, to the overheating and melting of fuel pins, formation and the evolution/motion of the molten pools, and finally, the failure of the hexcan surrounding the affected SA. Depending on the tightness of the upper plug, the transient goes on towards either possible dynamic or thermal propagations or both types of propagations of molten material into neighbour sub-assemblies. The physical models to describe the entire various transient are described as well as the experimental evidences from which they are derived. The perspectives in order to improve this tool are also underlined.

From the establishment of these physical models, 27 uncertain input parameters and their associated probability density functions are identified. Intermediate results obtained for a reference set of uncertain parameters are compared with a good agreement to available experimental results or numerical data. The propagation of input uncertainty has been performed via a Monte-Carlo sampling of 1000 simulations of the TIB simulator. From the elementary statistics of the corresponding predicted TIB outputs, the mean value for the final equivalent number of molten sub-assemblies is 5.5, with a standard deviation of 7.5. Even if in most cases a TIB would not exceed the safety criterion of 7 molten SAs, value assumed adequate for prevention of general core melting (Cadiou and Louvet, 2006 Bertrand and al. 2012), the probability of having this value upper than 7 is estimated to 18.1%.

Thanks to the low CPU cost of the TIB simulator, an uncertainty propagation study could have been carried out, providing a preliminary probabilistic safety analysis. In a similar way, sensitivity analyses have been performed and presented by (Marrel and Marie, 2014) in order to identify the most influential uncertain inputs for the different outputs of interest, like the final equivalent numbers of molten SAs and characteristic transient times.

## **Acknowledgment**

The authors would like to thank the Generation IV program of the industrial nuclear support and innovation Division of CEA which supports this work as well as the SFR R&D Project.

## **References**

- Alvarez, D., Malterre, P., Seiler, J.M., 1986. Natural convection in volume heated liquid pools – the BAFOND experiments: proposal for new correlations. Science and Technology of fast reactor safety, BNES, London.
- Bede, M., Perret, C., Pretrel, H., Seiler, J.M., 1993. One component, volume heated, boiling pool Thermohydraulics. 6th Topical International Meeting on Nuclear Reactor Thermal-Hydraulics (NURETH-6), Grenoble, France, October 5-8.

Corresponding author: [nathalie.marie@cea.fr](mailto:nathalie.marie@cea.fr)

Bernaz, L., 1999. Investigation of natural convection heat transfer to the cooled top boundary of a heated pool. 9th Topical International Meeting on Nuclear Reactor Thermal-Hydraulics (NURETH-9), San Francisco, California, October 3-9.

Bertrand, F., Bassi, C., Bentivoglio, F., Audubert, F., Guéneau, C., Rimpault, G., Journeau, C. 2012, Synthesis of the safety studies carried out on the GFR2400, Nuclear Engineering and Design 253 161–182.

Cadiou, T., Louvet J., 2006, Evaluation of the accident scenario initiated by a Total Instantaneous Blockage in a PHENIX subassembly, Nuclear Technology 153 256-263

Dadillon, J., Jamond, C., Sesny, R., Kayser, G., 1990. The SCARABEE Propagation Test Series PI-A and PV-A. 7<sup>th</sup> International Fast Reactor Safety Meeting, American Nuclear Society, 2, 187-196.

Der Kiuregian, A. 2007. Aleatory or epistemic? Does it matter? Special Workshop on Risk Acceptance and Risk Communication, Stanford University, March 26-27.

Duret, B., Bonnard, J.C., 1988. Crust Instability Criteria During Transient Freezing on a Liquid Film. Proceedings of the ASME Winter *Annual Meeting*, Chicago, Illinois, Nov. 27-Dec. 2.

Fast Reactor Database, 2006. IAEA-TECDOC-1531, update.

Gentle, J.E., 2003. Random number generation and Monte Carlo methods. Springer.

Iooss, B., Gaudier, F., Marques, M., Spindler, B., Tourniaire, B., 2009. Uncertainty assessment in severe nuclear accident scenarios. First International Conference on Advances in System Simulation 2009, 94-99.

Kayser, G., Charpenel, J., Jamond, C., 1998. Synthesis of SCARABEE-N program, with main results and application to the total instantaneous blockage reactor. Nuclear Engineering and Design, 128, 144-185.

Kayser, G., Soussan, P., 1991. Propagation and freezing in SCARABEE. 14th meeting of the LMBWG, ENEA Brasimone, April 16-18th.

Kondo, Sa., Morita, K., Tobita, Y., Kamiyama, K., Brear, D.J., Fischer, E.A., 1996. SIMMER-III : A computer program for LMFR core disruptive accident analysis. PNC ZN9410 96-207, O-arai Engineering Center, Power Reactor and Nuclear Fuel Development Corporation.

Livolant, M., Dadillon, J., Kayser, G., Moxon, D., 1990. SCARABEE : a test reactor and programme to study fuel melting and propagation in connexion with local faults, objectives and results. Int. fast Reactor Safety meeting, Snowbird, Utah, 2, 177-186.

Luck, L., Bell, C., 1985. The case of integral core – disruptive accident analysis. ANS/ENS fast reactor safety meeting, Knoxville, TN, USA, April 21.

Lyon, R.N., 1949. Heat transfer at high fluxes in confined spaces. PhD thesis, University of Michigan, Ann Arbor, Mich.

Corresponding author: nathalie.marie@cea.fr

Mercier, P., 1978. Sodium boiling two phase flow investigations by forced convection in single channel. 8th Liquid Metal Boiling Working Group Meeting, Mol, Belgium, October 11-13.

Marrel, A., Marie, N., De Lozzo, M., 2015. Advanced Surrogate model and sensitivity analysis methods for SFR accident assessment. Reliability Engineering and System Safety 138 232-241.

Martin, F.J., 1980. Bottled transition phase analysis. Preliminary report. HEDL-TME. 78-64.

Nakai, R., Suzuki, T., Yamano, H., Seino, H., Ishikawa, H., 2009. Development of Severe Accident Evaluation Technology (Level 2 PSA) for Sodium-cooled Fast Reactor (1) Overview of evaluation Methodology Development. ICAPP'09, Tokyo, Japan, May 10-14.

Papin, J., 2012. Behavior of Fast Reactor Fuel During Transient and Accident Conditions. Comprehensive Nuclear Materials, Elsevier Ltd.

Papin, J., Sesny, R., Soussan, P., Mac Dougall, J., 1990. The SCARABEE Total Blockages Test Serie: Synthesis of the interpretation. 7<sup>th</sup> International Fast Reactor Safety Meeting, American Nuclear Society, 1, 367-376.

Papin, J., Seiler, J.M., 1983. Synthesis of clad motion experiments interpretation: codes and validation. 2nd International Topical Meeting on Nuclear Reactor Thermal Hydraulics, Santa Barbara (California), January 11-14.

Ravi, L., Velusamy, K., Chellapandi, P., 2013. A robust thermal model to investigate radial propagation of core damage due to total instantaneous blockage in SFR fuel assembly. Annals of Nuclear Energy, 62, 342-356.

Seiler, J.M., 1977. Etude de l'ébullition du sodium au cours d'une excursion de puissance en géométrie monocanal. Thèse de Docteur Ingénieur, USM Grenoble.

So, D.S., Seiler, J.M., 1984. Sodium boiling, dry out and clad melting in a sub-assembly of LMFBR during a Total and Instantaneous inlet blockage accident. 11<sup>th</sup> Liquid Metal Boiling Working Group, Grenoble 23-26 October 1984

Yamano, H., Sato, I., Tobita, Y., 2012. Development of technical basis in the initiating and transition phases of unprotected events for Level-2 PSA methodology in sodium-cooled fast reactors. Nuclear Engineering and Design, 249, 212-227.